The photoelectron spectrum of elusive cyclic-N_3 and characterization of the potential energy surface and vibrational states of the ion

Dmitri Babikov[a)]
Chemistry Department, Marquette University, Milwaukee, Wisconsin 53201-1881

Vadim A. Mozhayskiy and Anna I. Krylov
Department of Chemistry, University of Southern California, Los Angeles, California 90089-0482

(Received 16 May 2006; accepted 13 July 2006; published online 24 August 2006)

A potential energy surface is constructed for the ground $X\ ^1A_1$ electronic state of cyclic-N_3^+ based on three-dimensional spline interpolation of *ab initio* points. The vibrational states of this molecular ion are calculated in the range up to 14 500 cm^{-1} using hyperspherical coordinates and the coupled-channel (sector-adiabatic) approach. All the vibrational states are analyzed and assigned. The Franck-Condon overlaps of these states with the vibrational states of the neutral are calculated to predict the photoelectron spectrum of cyclic-N_3. Peak intensities are governed by the nodal structure of the vibrational wave functions and reflect the large geometric phase effect predicted for cyclic-N_3. Experimental validation may shed light on the existence of this elusive molecule and confirm the magnitude of the geometric phase effect. © *2006 American Institute of Physics*.
[DOI: 10.1063/1.2335437]

I. INTRODUCTION

Cyclic-N_3 is a Jahn-Teller molecule that exhibits a conical intersection between its two lowest potential energy surfaces (PESs) at D_{3h} (equilateral triangle) configurations. The Jahn-Teller distortions lead to a lower-symmetry equilibrium geometry, i.e., three equivalent C_{2v} (isosceles triangle) minima connected by pseudorotation motion. At the point of conical intersection the symmetry of the Born-Oppenheimer electronic wave function changes from $^2B_1$ to $^2A_2$ which imposes additional conditions on nuclear wave functions.

Cyclic-N_3 was first detected in the UV photolysis experiments:[1–3]

$$ClN_3 \xrightarrow{h\nu} Cl + N_3. \tag{1}$$

Using the velocity map imaging technique the kinetic energy distribution of N_3 fragments was obtained, which also provided a low-resolution spectrum of the internal energy in the N_3 molecules. The distribution had pronounced bimodal structure and clearly indicated that, in addition to the already known weakly bound linear-N_3 isomer, there was another energetic form of N_3, with energy about 1.35 eV above that of linear N_3. This finding was in good agreement with earlier *ab initio* calculations,[4] which predicted a metastable ring isomer in the form of an acute isosceles triangle (cyclic-N_3) at 1.30 eV above linear N_3.

Thus, cyclic-N_3 carries a large amount of energy and is an interesting new candidate for technological applications in energy storage, high nitrogen explosives, and new propellants. It is worth mentioning that the nitrogen resources on our planet are practically limitless. Moreover cyclic-N_3 could be used as a powerful and clean monopropellant:

$$2N_3 \rightarrow 3N_2. \tag{2}$$

Since this reaction produces only nitrogen molecules, the main component of atmospheric air, the exhaust gases present no environmental hazards and are indistinguishable from the ambient air.

The first experiments[1–3] stimulated much interest from the theory side. Extensive electronic structure calculations of the critical points on global PES for nitrogen triatomic have been carried out.[5] It was demonstrated that cyclic-N_3 represents stable species, at least in a gas-phase collision-free regime (e.g., in molecular beams). This N_3 isomer is "locked" in a deep potential energy well surrounding the $^2A_2/^2B_1$ conical intersection; the barriers to isomerization into linear N_3 and to dissociation onto $N(^2D)+N_2$ products are 31.9 and 33.1 kcal/mol, respectively. Dissociation onto the ground state products $N(^4S)+N_2$ is spin forbidden and can proceed only through the three intersystem crossings located at energies above 28.3 kcal/mol, which was shown to be inefficient. An accurate *ab initio* potential energy surface for cyclic-N_3 has been computed[6] and rigorous calculations of the vibrational states have been performed taking into account the geometric phase effect.[7] Thermodynamics of the cyclization mechanism has also been explored.[8] On the experimental side, new evidence for production of cyclic-N_3 has been discovered in the ClN_3 photofragment translational spectroscopy experiments,[9] in the experiments on photoionization of N_3 fragments using the synchrotron radiation source,[10] in the time-of-flight studies of HN_3,[8] and finally in the recent velocity map imaging experiment.[11] For the comprehensive review of the experimental and theoretical work on cyclic-N_3 see Ref. 12.

All available experimental information for cyclic-N_3 is consistent with the theoretical picture of this molecule, however, the final proof for the existence of cyclic-N_3 is yet to be

[a)]Author to whom correspondence should be addressed. Electronic mail: dmitri.babikov@mu.edu

made by means of high-resolution spectroscopy. Two possibilities have been discussed at the recent meetings, one being the infrared spectroscopy[13] and the other one the photoelectron spectroscopy. The latter requires information about the ionic cyclic-N_3^+ species, e.g., ionization potential, as well as PES of the ground and electronically excited states of cyclic-N_3^+. These topics have been addressed in our recent work[14] and have indicated a favorable path to experimental implementation. Here we present calculations of the vibrational wave functions of cyclic-N_3^+ and the photoelectron spectrum of the neutral.

Recently, several studies of the molecules that are somewhat similar to cyclic-N_3 have been published. For example, an old interest[15–18] in the simplest members of this family, H_3^+ and its isotopologue D_3^+, has been revived by significant progress in theoretical treatment of the recombination reaction relevant to interstellar chemistry: $H_3^+ + e \rightarrow H_3 \rightarrow H_2 + H$ (dissociative electron capture).[19–21] An impressive experimental and theoretical work has been published on high-resolution spectroscopy of Li_3,[22,23] where both the initial (ground $X\,^2E'$) and the final (excited $A\,^2E''$) electronic adiabatic surfaces constitute the doubly degenerate Jahn-Teller pairs. In this system, the inclusion of the geometric phase effects for both surfaces is necessary for accurate calculations of the vibrational states and predictions of the spectra. Rotationally resolved electronic spectrum of cyclic-B_3 has also been observed experimentally;[24] however, in this molecule only the excited state ($2\,^2E'$) is a Jahn-Teller pair. Furthermore, very low stabilization energy in PES of this state results in very small Jahn-Teller distortion from the D_{3h} configuration, which therefore can be neglected in an approximate treatment. A neighbor of nitrogen in the periodic table, carbon, also has an energetic cyclic-C_3 form ($^3A_2$), which exhibits no conical intersection in the D_{3h} and is an equilateral triangle[25] with a simple vibrational spectrum. A cyclic trimer has also been predicted and theoretically characterized for another neighbor of nitrogen, oxygen. The energetics of cyclic-O_3 is very similar[26,27] to that of the cyclic nitrogen, although it has an equilibrium D_{3h} structure and exhibits no conical intersections in the ground $2\,^1A_2$ state. Note that cyclic-O_3 has never been observed in the gas-phase experiment due to negligible Franck-Condon overlap with the ground state of the "open" ozone molecule. Many references to earlier works on Na_3, Cu_3, and Al_3 can be found in the above papers as well.

Several special features distinguish cyclic-N_3 from all these molecules. For example, this is the only known homonuclear triatomic molecule with a vibrational zero-point energy (ZPE) significantly higher than the energy of the pseudorotation barrier and significantly lower than the energy of the conical intersection.[5,6] Due to these properties, the geometric phase effects are very large for all the vibrational states of cyclic-N_3 (including the ground vibrational state) and can be investigated by performing calculations on a single adiabatic potential energy surface,[7] i.e., without taking into account nonadiabatic interactions with the cone states, which are important in the vicinity of the conical intersection. Moreover, in the photoionization of cyclic-N_3, the initial state is a Jahn-Teller state while the final state is not, which is different from examples discussed in the previous paragraph. Thus, the complicated Jahn-Teller wave functions of cyclic-N_3 are projected onto simpler wave functions of cyclic-N_3^+, which makes signature of geometric phase effects very clear. However, higher excited states of cyclic-N_3^+ (in the range of 5–8 eV above the ground electronic state) exhibit conical and glancing intersections[14] and offer many more opportunities for experimental and theoretical studies.

The structure of the paper is as follows. In Sec. II we describe the theoretical approach and computational details. The results are presented and discussed in Sec. III. Conclusions are given in Sec. IV.

II. THEORETICAL AND COMPUTATIONAL METHODS

A. Coordinates, *ab initio* method, and spline interpolation of PES

As in the earlier work,[6,7] we describe the positions of nitrogen nuclei in the cyclic-N_3^+ triatomic using *adiabatically adjusting principal-axes hyperspherical* (APH) coordinates.[28,29] In terms of the usual mass scaled internal Jacobi coordinates (r, R, α), the APH coordinates (ρ, θ, ϕ) are defined as follows:

$$\rho = \sqrt{R^2 + r^2}, \quad \rho \in [0;\infty]; \tag{3}$$

$$\tan\theta = \frac{\sqrt{(R^2 - r^2)^2 + (2Rr\cos\alpha)^2}}{2Rr\sin\alpha}, \quad \theta \in [0;\pi/2]; \tag{4}$$

$$\tan\phi = \frac{2Rr\cos\alpha}{R^2 - r^2}, \quad \phi \in [0;2\pi]. \tag{5}$$

Qualitatively, the value of the hyper-radius ρ is a measure of the overall "size" of a triatomic molecule. Hyperangles θ and ϕ describe changes in its "shape."

Stereographic projection[28] is often used with the APH coordinates because this is a convenient way to plot a two-dimensional (2D) slice of PES at a fixed value of the hyper-radius ρ, while θ and ϕ are allowed to vary. This corresponds to variation of the shape of the triatomic molecule keeping its overall size constant. In such a 2D plot, the energy is a function of two Cartesian variables X and Y defined as

$$X = \cos\phi\tan(\theta/2), \tag{6}$$

$$Y = \sin\phi\tan(\theta/2), \tag{7}$$

where $-1 \leqslant X \leqslant 1$, $-1 \leqslant Y \leqslant 1$. With this choice, the center of the plot ($X=0$, $Y=0$) corresponds to $\theta=0$ and describes the triatomic in D_{3h} geometry, the equilateral triangle. A distance of any point from the center of the plot is determined by the variable θ only:

$$\sqrt{X^2 + Y^2} = \tan(\theta/2). \tag{8}$$

Points at the unit circle $X^2+Y^2=1$ correspond to $\theta=\theta_{\max}=\pi/2$ and describe linear configurations of the triatomic system (not considered here). Stereographic projections at various values of the hyper-radius ρ can be stacked together to give a useful three-dimensional (3D) view of PES (Ref. 6) or of the wave functions.[7]

Using APH coordinates, we have set up a dense grid in three dimensions with ρ(a.u.)={2.91;2.99;3.065;3.14; 3.205;3.268;3.325;3.40;3.485;3.6;3.725;3.86}, $\tan(\theta/2)$ ={0.0;0.022;0.047;0.078;0.111;0.149;0.19;0.25}, and ϕ ={0;15°;30°;45°;60°}. Our grid contains only five equidistant points in ϕ because PES is quite smooth along this coordinate and the energy varies slowly as the observer goes around the origin. Actually, in the vicinity of the origin (i.e., near the equilateral configuration), PES is almost isotropic in ϕ, which results in a near degeneracy between two vibration modes in this and some other D_{3h} triatomic molecules.[24–27] This feature will be discussed below. Along θ and ρ, the energy of cyclic-N_3 changes significantly and we had to develop a much denser nonregular grid for these two coordinates. First, we performed calculations of a few points along the D_{3h} and C_{2v} symmetry lines to determine a coarse topology of the surface, and then we built a full 3D grid for accurate representation of the surface in (ρ,θ,ϕ) space. Our grid contains 12 points along the $\theta=0$ line to describe equilateral triangle configurations (D_{3h}). The $12\times7\times2=168$ points in the $\phi=0$ and $\phi=60°$ planes are used to describe isosceles configurations (C_{2v}) while the $12\times7\times3=252$ points are used to describe cyclic-N_3^+ configurations of the general C_s symmetry. Thus, our grid contains a total of 432 points. Electronic structure calculations[14] for cyclic-N_3^+ were carried out at each point of this grid. The PES points are given as EPAPS supplement.[36] Single point energies of the ground and 12 lowest excited electronic states of cyclic-N_3^+ were obtained at the CCSD/cc-pVTZ and EOM-CCSD/cc-pVTZ levels of theory,[30–33] respectively, with 1*s* core orbitals frozen using Q-CHEM *ab initio* package.[34] The quality of the potential energy surface for closed shell N_3^+ near the equilibrium can be evaluated based on typical errors of CCSD/cc-pVTZ for frequencies: the mean absolute errors of the CCSD/cc-pVTZ harmonic frequencies and anharmonic constants are about 60 cm^{-1} (1.5%–3%) and 1.7 cm^{-1}, respectively.[35]

Finally, an accurate three-dimensional interpolant between the *ab initio* points has been constructed using the tensor product *B*-cubic spline representation.[37] The resulting PES thoroughly covers the energy range up to 2 eV ($\sim$16000 cm^{-1}), which is significant for calculations of the vibrational states of cyclic-N_3^+ seen in both cold and hot photoelectron bands of the neutral. Within the configuration space covered by the interpolant on the 3D grid, the surface representation is very accurate. In addition, we have constructed a one-dimensional (1D) extrapolant along θ coordinate into the region outside of the grid, i.e., behind the value of $\tan(\theta/2)=0.25$, using a simple quadratic function. PES is not accurate in that region, but this smooth extension was necessary for the finite-basis representation (FBR)/discrete variable representation (DVR) calculations of the vibrational states. Extrapolation in ϕ coordinate is unnecessary; due to periodicity all physical values of ϕ are covered by the grid.[28] Extrapolation in the hyper-radius ρ is not required either, because the relevant range of ρ, to be scanned by the sector-adiabatic approach,[29] is thoroughly covered by the grid.

B. Calculations of the vibrational states

It is often assumed that PES of the D_{3h} molecules is isotropic along ϕ and that the motion in the (θ,ϕ) plane is uncoupled from the breathing motion characterized by ρ. No experimental information on cyclic-N_3^+ is currently available to support these approximations. In contrast, some inter- and intramode anharmonicities (couplings) are apparent from just looking at the PES pictures. For example, in Fig. 2 in the next section, the contour lines look very similar to circles near the origin (small θ); however, they distort quite significantly towards the triangular shape at larger values of θ. Thus, the potential energy surface $V(\rho,\theta,\phi)$ appreciably couples different internal degrees of freedom, and the Schrödinger equation for nuclear motion is nonseparable and cannot be solved by analytical decoupling. Therefore, we carried out the numerically accurate full dimensional calculations of the vibrational states including all couplings and anharmonicities present in PES.

We "decouple" the radial and angular coordinates numerically using the sector-adiabatic technique.[29] In this approach, the full dimensional Schrödinger equation is solved in two steps. First, the hyper-radius ρ is partitioned into a large number of sectors (intervals) and the two-dimensional angular (θ,ϕ) part of the equation is solved numerically for each sector with $\rho=\rho_\xi$ fixed (as a parameter) at the center of each sector. The potential coupling matrices and overlap matrices between the neighboring (adjacent) sectors are also computed at this step. In the second step, a set of one-dimensional coupled-channel (CC) equations is obtained for the hyper-radial ρ coordinate[29] and is solved using a numerical propagation technique. In this procedure, the coupling is recovered and the accurate full dimensional solutions of the Schrödinger equation are obtained using the exact Hamiltonian and including all couplings.

The parallel computer code of Kendrick,[38–40] which we applied previously to calculate the vibrational bound states in the cyclic-N_3 molecule,[7] was used in this work as well. The code employs an efficient hybrid FBR/DVR (Ref. 41) algorithm to solve the angular (θ,ϕ) part of the problem and uses Numerov propagator[42] to solve the coupled-channel equations in ρ. Propagation of the coupled-channel equations is performed separately for the states of different symmetries. The range of ρ (a.u.) $\in[2.91;3.86]$ was partitioned onto 155 sectors using a constant step size of $\Delta\rho=0.006$ a.u. Dimension of the DVR in θ based on Jacobi polynomials was $N_\theta=104$, which corresponds to the number of Gauss-Legendre quadrature points in $\tilde{\theta}\equiv\pi-2\theta$. The FBR in ϕ uses complex exponential functions and its basis set size was $N_\phi=165$. The cutoff value for the sequential diagonalization truncation (SDT) algorithm was ρ dependent and varied from at 20 eV at small ρ to 7.2 eV near the minimum point and to 9 eV at large ρ. The coupled-channel equations in ρ contained 40 channels for A_1- and A_2-symmetry solutions and 160 chan-

nels (80 doubly degenerate channels) for E-symmetry solutions. Convergence studies were performed with respect to the covered range of ρ, the number of sectors in ρ, the energy cutoff values, the 2D basis set size in θ and ϕ, the number of coupled channels, and the accuracy of Numerov bisections. The convergence of all states of A_1 and A_2 symmetries and most E-symmetry states is below 1 cm^{-1}. Most of the states below 10 000 cm^{-1} are converged tighter than 0.1 cm^{-1}. Several E-symmetry states did not converge better than to within 5 cm^{-1}.

Since cyclic-N_3^+ contains three identical nuclei, the symmetry of its vibrational eigenfunctions can be classified using the irreducible representations (irreps) of the permutation group S_3. This group has two nondegenerate irreps, A_1 and A_2, and one doubly degenerate irrep, E. In the APH coordinates, the symmetry is entirely determined by the behavior of the wave function along the hyperangle ϕ that encircles the origin. The vibrational wave functions of the A_1 (A_2) symmetry are symmetric (antisymmetric) with respect to an exchange of any two of the three nuclei and thus exhibit a threefold symmetry. These symmetry operations correspond to reflections of the wave functions through the three C_{2v} planes, which appear in the APH coordinates at $\phi=0$, $\phi=120°$, and $\phi=240°$ and cross along the D_{3h} line which appears in the APH coordinates at $\theta=0$ (see Fig. 2 below). The wave functions of E states exhibit twofold symmetry; in each pair of the doubly degenerate wave functions, one (E_a) is symmetric with respect to reflection through the $\phi=0°$ plane and another one (E_b) is antisymmetric. Classification of the vibrational states according to A_1, A_2, and E symmetries is exact.

C. Modeling of the photoelectron spectrum

In a photoexcitation process, the intensities of spectral peaks are determined by squares of the dipole moment matrix elements between the initial and final states:[43]

$$I_{\text{photo}} \propto |\langle \psi_f | \boldsymbol{\mu}_{f,i} | \psi_i \rangle_{\rho,\theta,\phi}|^2 \approx |\boldsymbol{\mu}_{f,i}(\rho_{\text{eq}}, \theta_{\text{eq}}, \phi_{\text{eq}})|^2 \langle \psi_f | \psi_i \rangle^2_{\rho,\theta,\phi}, \quad (9)$$

where $\psi(\rho,\theta,\phi)$ and $\boldsymbol{\mu}_{f,i}(\rho,\theta,\phi)$ represent the vibrational wave functions and the dipole moment vector function, respectively; integration is over the vibrational coordinates only. The second expression assumes that each component of $\boldsymbol{\mu}_{f,i}$ can be approximated by its value at the equilibrium nuclear configuration: $\boldsymbol{\mu}_{f,i}(\rho,\theta,\phi) \approx \boldsymbol{\mu}_{f,i}(\rho_{\text{eq}}, \theta_{\text{eq}}, \phi_{\text{eq}})$. This standard approximation (i.e., Condon approximation) is applicable to molecules with the ground vibrational wave function *localized* (i.e., as a multidimensional Gaussian function) near the equilibrium position $(\rho_{\text{eq}}, \theta_{\text{eq}}, \phi_{\text{eq}})$. The ground vibrational state $(0,0^0)$ of cyclic-N_3^+ (described in the next section) is a good example of this kind. In contrast, the ground state wave function of neutral cyclic-N_3, which plays the role of $\psi_i(\rho,\theta,\phi)$ in our case, is highly *delocalized*. This wave function is shown in Fig. 1, lower frame, using isovalue surface for $|\psi|^2$ in three dimensions. PES of cyclic-N_3 is shown in Figs. 2–4 (lower frame) and will be discussed in detail in the next section. Analysis of PES and the wave function shows that it is still possible to define $\rho_{\text{eq}}=\rho_{\text{MIN}}$ (see Fig. 4 below) and, as an approximation of some sort, to choose θ_{eq} to be somewhere between θ_{MIN} and θ_{TS}, because these numbers are quite close (see Fig. 3 below), however, there is no representative value of the hyperangle ϕ that can serve as ϕ_{eq}. Rigorously speaking, we cannot define $\phi_{\text{eq}}=\phi_{\text{MIN}}$ because the minima on cyclic-N_3 PES are very shallow and, consequently, the wave function is not localized in these minima. A more appropriate strategy, perhaps, would be to develop an approximation of another kind, where the isotropic behavior of $\psi_i(\rho,\theta,\phi)$ along the hyperangle ϕ is assumed, based on the fact that the shape of PES along this coordinate is more like in the particle on the ring (see Fig. 2) rather than in the harmonic oscillator problem. However, such a model would *not* be applicable to cyclic-N_3 and other Jahn-Teller molecules, where $\boldsymbol{\mu}_{f,i}(\rho,\theta,\phi)$ has strong ϕ dependence. This phenomenon is known as the geometric phase effect or the Berry phase.[44–46] In the calculations of the vibrational wave functions it can be accounted for either by specifying the double-valued boundary conditions and using half-integer basis set for FBR in ϕ,[22,23,47,48] or by employing a more general gauge theory.[49–52] In the previous work[7] on cyclic-N_3, we followed the latter approach, although both methods produce the vibrational wave functions with correct permutation symmetries (A_1, A_2, or E) that are also consistent with the symmetry of $\boldsymbol{\mu}_{f,i}(\rho,\theta,\phi)$. This is important because the selection rules are determined by symmetry properties of the initial and final wave functions in Eq. (9): $A_1' \to A_1''$, $A_2' \to A_2''$, and $E' \to E''$, where $'$ and $''$ are used to label the states of cyclic N_3 and N_3^+, respectively. Note that

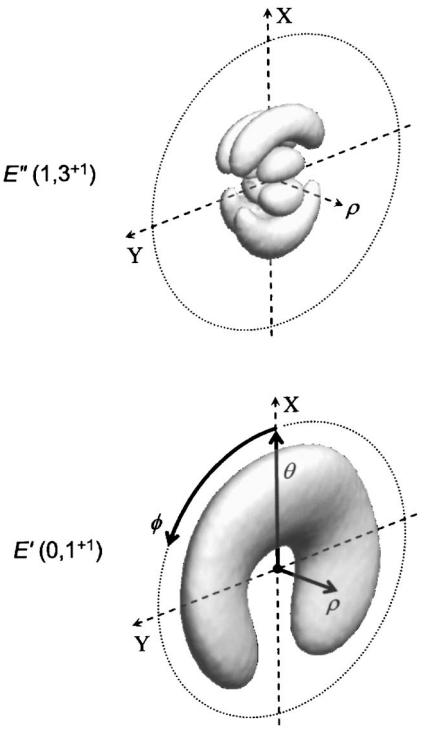

FIG. 1. 3D wave functions for the ground vibrational state of cyclic-N_3 with the geometric phase included (the "horseshoe-type" state, lower frame) and the brightest state of cyclic-N_3^+ in the photoelectron spectrum (upper frame). Assignments are given in terms of vibrational polyads (v_1, v^{ℓ}). The hyperradial direction ρ is plotted perpendicularly to the (X,Y) plane. For simplicity of presentation, the $\tan(\theta/2)$ axis is labeled by the polar hyperangle θ throughout the paper.

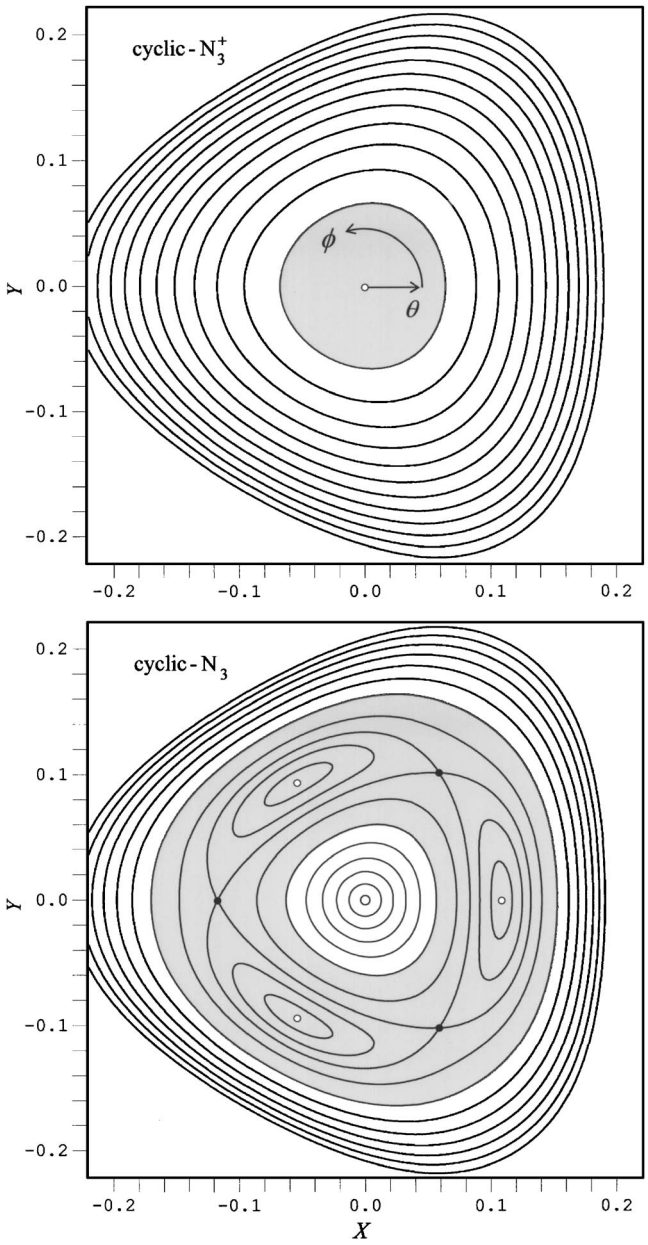

FIG. 2. Contour maps of the potential energy surfaces for neutral cyclic-N_3 (lower frame) and ionic cyclic-N_3^+ (upper frame). Stereographic projections discussed in the text are used at ρ=3.466 a.u. and ρ=3.268 a.u. for cyclic N_3 and N_3^+, respectively, which corresponds to the minimum energy points for each species. Shaded areas show zero-point energies for each species. In the lower frame the conical intersection is in the middle (X=0, Y=0); empty dots (◦) indicate points of minima, filled dots (•) indicate transition state points. Note that energies of the contour lines are different in the two frames. In the lower frame: 0.005, 0.02, and 0.0409, then from 0.08 with 0.08 steps until 0.64 eV. In the upper frame: from 0.24 with 0.24 steps until 2.88 eV.

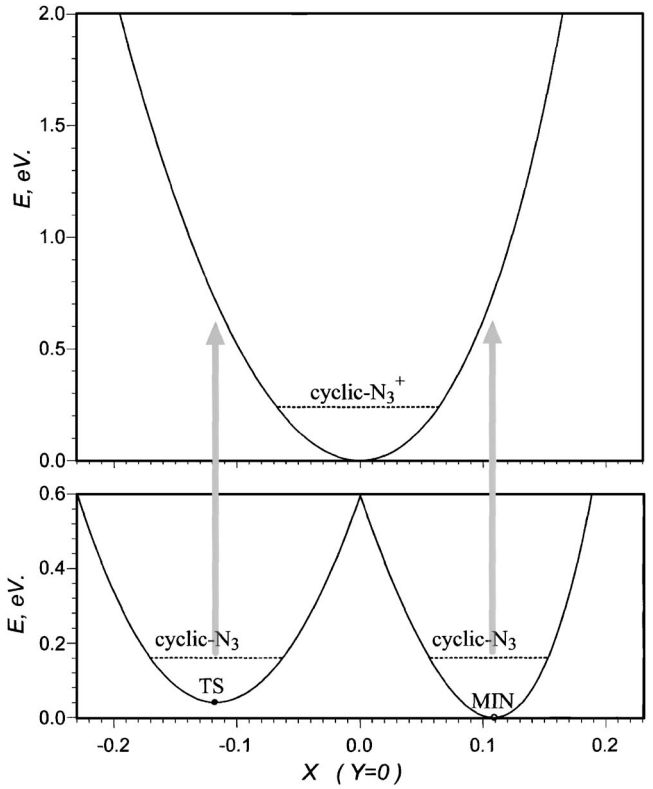

FIG. 3. 1D slices through the Y=0 (horizontal) line of the 2D plots given in Fig. 2. Zero-point energies of the two species are shown using dashed lines. It is clear that the transition state (TS) energy in cyclic-N_3 is only slightly above the minimum energy point (MIN) and is small compared to its zero-point energy. Photoionization process leading from cyclic-N_3 to cyclic-N_3^+ is shown schematically by two gray arrows. Note that the energy scales in the upper and lower frames are different.

since the ground electronic state wave function of cyclic-N_3^+ is a fully symmetric ($X\,^1A_1$) and single-valued function of the nuclear coordinates (ρ, θ, ϕ), no geometric phase effect is present in the ion and the symmetry treatment of its vibrational states $\psi_f(\rho, \theta, \phi)$ is straightforward.

Therefore, for the exact calculation of the photoelectron intensities, one should first calculate $\boldsymbol{\mu}_{f,i}(\rho, \theta, \phi)$ in all the regions of the configuration space spanned by the vibrational wave functions $\psi_i(\rho, \theta, \phi)$. Then, one should calculate the overlaps $\langle \psi_f | \boldsymbol{\mu}_{f,i} | \psi_i \rangle_{\rho,\theta,\phi}$ from Eq. (9) properly accounting for the geometric phase in ψ_i and $\boldsymbol{\mu}_{f,i}$. A similar approach (although without geometric phases) is common in infrared vibrational spectroscopy, however, it is rarely employed in the electronic spectroscopy, and almost never in photoelectron spectroscopy because of the additional complexity due to outgoing free electron, and is beyond the scope of the present paper. The correct treatment of the geometric phases of cyclic-N_3 is readily available, since the vibrational wave functions $\psi_i(\rho, \theta, \phi)$ with correct permutation symmetry and with the geometric phases included were characterized in the previous work.[7] However, the dipole moment function $\boldsymbol{\mu}_{f,i}(\rho, \theta, \phi)$ from Eq. (9) is not yet available and we employ a less rigorous Condon-type procedure, that is, we simply calculate the Franck-Condon (FC) overlaps $\langle \psi_f | \psi_i \rangle_{\rho,\theta,\phi}$ of Eq. (9) to predict the intensities.

For cyclic-N_3^+, we use the vibrational wave functions calculated in this work (see next section). For the neutral, we employ the vibrational wave functions calculated in the previous work[7] with the geometric phase included using the gauge theory. Readers are encouraged to read Ref. 7, where the importance of the geometric phase effect in the vibrational spectra of cyclic-N_3 has been demonstrated.[7,53] For example, in the absence of the geometric phase, the ground vibrational state is always totally symmetric A_1 state and the first vibrationally excited state is of E symmetry. In the cyclic-N_3, due to the geometric phase, the lowest state of E

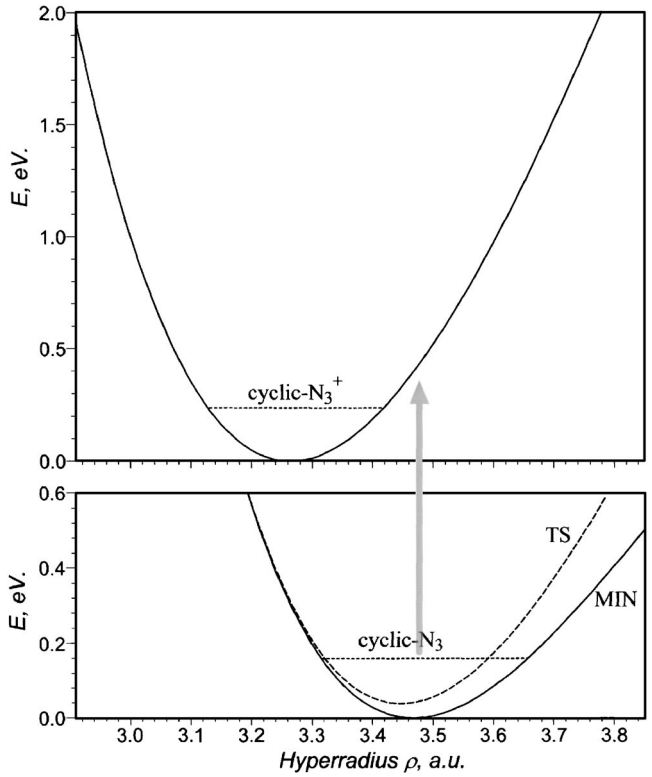

FIG. 4. Potential energy for the critical points of the two species as a function of the hyper-radius. Energy scales, zero-point energies, and photoionization process are shown as in Fig. 3. The Franck-Condon region is clearly seen.

symmetry is pushed down to 1325.67 cm^{-1} and becomes the ground vibrational state, while the lowest state of A_1 symmetry is lifted up to 1401.22 cm^{-1} and becomes the first excited vibrational state.[7] This feature is of major importance for spectroscopy of cyclic-N_3, as it determines that the main (cold) band will be due to $E' \rightarrow E''$ transitions, while the hot band will be due to $A_1' \rightarrow A_1''$ transitions.

Although the cyclic-N_3 molecules are produced rotationally cold in the recent molecular beam experiments,[1–3,9–11] their vibrational temperature appears to be high, about 300 K, because there is no vibrational relaxation following the photodissociation of ClN_3. At this temperature, a few more low lying vibrational states of cyclic-N_3 are populated and may appear as hot bands in the photoelectron spectrum. For example, the third vibrational state of cyclic-N_3 is only at 1501.68 cm^{-1}. This state is the lowest state of A_2 symmetry. Photoionization from this state will give rise to a progression of the $A_2' \rightarrow A_2''$ transitions, although those must be much less intense due to small nuclear spin weight of A_2 symmetry (see below). The fourth vibrational state in cyclic-N_3, another state of E symmetry at 1668.88 cm^{-1}, should also be taken into account. The populations of all higher states are insignificant (i.e., less then 5% of the ground vibrational state population at 300 K), and therefore, these states are not included in calculations.

In addition to thermal Boltzmann distribution, we also included nuclear spin degeneracy factors. The nitrogen nuclei are spin-one bosons and the total number of nuclear spin states is given by $(2s+1)^3=27$ for $s=1$. Among them, there are $(2s+1)(2s+3)(s+1)/3=10$, $(2s+1)(2s-1)s/3=1$, and $(2s+1)(s+1)8s/3=16$ states of A_1, A_2, and E symmetries, respectively. Since the total wave function must be symmetric, the nuclear spin states should be combined with vibronic states of the same symmetry. Thus, the numbers 10, 1, and 16 should be used as weighting factors for the bands of these symmetries. Since E-symmetry states occur in doubly degenerate pairs (E_a and E_b), the FC factors for the $E' \rightarrow E''$ transitions should be summed over the final states (E_a'' and E_b'') and averaged over the initial states (E_a' and E_b'). Using the orthogonality of E_a and E_b states, we obtain the FC factors for $E' \rightarrow E''$ transitions:

$$\mathrm{FC} = \frac{\langle E_a''|E_a'\rangle^2 + \langle E_b''|E_b'\rangle^2}{2}. \tag{10}$$

Rotational broadening was not included in the calculations.

III. RESULTS AND DISCUSSION

A. Potential energy surface of cyclic-N_3^+

This section presents PES of cyclic-N_3^+, discusses its major features, and compares this surface to the surface of the neutral cyclic-N_3. We employ 2D and 1D slices through the hypersphere. Figure 2 shows the two-dimensional (θ, ϕ) slice through the minimum energy point for each surface; the stereographic projection described above is used. Several differences between the two species are clearly seen: Neutral cyclic-N_3 is a Jahn-Teller molecule, which exhibits *conical intersection* at D_{3h} (Fig. 2, lower panel), 4568 cm^{-1} above the minimum. In contrast, PES of cyclic-N_3^+ has a *minimum* at D_{3h} configuration (upper panel of Fig. 2). These features persist for all values of the hyper-radius ρ. In the ionic D_{3h} species, the equilibrium lengths of the three equivalent nitrogen-nitrogen bonds are equal to 1.313 Å.[14] In contrast, the minimum energy point of the neutral species is shifted to an acute isosceles triangle geometry with the apex angle of 49.86°, two longer bonds of 1.466 Å each, and one shorter 1.236 Å bond.[5,6] Three such equivalent minima exist on PES; they correspond to placing each of the three nitrogen atoms of this molecule in the apex position. The wells around these minima (shown in Fig. 2) are very shallow and are separated by three transition states at 311.33 cm^{-1}. At these transition state points, cyclic-N_3 is an obtuse isosceles triangle with the apex angle of 71.93°, two shorter bonds of 1.306 Å each, and one longer 1.535 Å bond.[5,6] Note that all geometries of an X_3 triatomic molecule that belong to the C_{2v} point group (isosceles triangles) appear in the APH coordinates at $\phi = n \times 60°$ (n is an integer). The points at $\phi = \{0; 120°; 240°\}$ represent the acute isosceles triangle geometries (including the three minima), while the points at $\phi = \{60°; 180°; 300°\}$ represent the obtuse isosceles triangle geometries (including the three transition states).

Shaded areas superimposed with the contour plots in Fig. 2 accentuate those parts of the surfaces that lie below the corresponding zero-point energies, i.e., 1325.67 and 1927.48 cm^{-1} for cyclic N_3 and N_3^+, respectively. These areas can be described as two-dimensional classically allowed regions for the ground vibrational states. The readers can clearly see that the permutation of the three nuclei in cyclic-

N_3, the so-called pseudorotation, is accessible at zero-point energy, as all the minima and the transition states fall into the shaded area. Also, since the overlap between the shaded areas from the two frames is negligible, the Franck-Condon factors between the ground vibrational states of the neutral and ionic species are relatively small, but increase rapidly with vibrational excitation.

Additional insight is obtained by looking at the slice along the $Y=0$ lines of the pictures from Fig. 2, which are shown in Fig. 3 for both the neutral and ionic species. This picture further emphasizes the efficiency of the pseudorotation in cyclic-N_3, which occurs well above the transition states. Moreover, it is clear that the minimum and the transition state point of neutral's PES occur at slightly different values of the hyperangle θ: $\theta_{MIN} \neq \theta_{TS}$. This picture also addresses a common misconception related to photoexcitation (including photoionization) processes in the triatomic Jahn-Teller molecules,[54,55] i.e., by looking only at Fig. 3, one could decide that the two "minima" on the left and right sides of the conical intersection represent two different isomers with somewhat different zero-point energies. Consequently, one could erroneously expect that the photoelectron spectrum should reflect this difference in the form of the spectral peak splittings. This is certainly incorrect because, as one can clearly see from Fig. 2, the critical point on the left side of the conical intersection is a transition state rather than a minimum. Besides, in cyclic-N_3, due to the relatively low transition states and high zero-point energy, each vibrational wave function is highly delocalized along the hyperangle ϕ (see Fig. 1) and has nonzero density almost everywhere around the conical intersection[7] (except the symmetry imposed nodes). In fact, the zero-point energy lines on both sides of the conical intersection (Fig. 3, lower panel) belong to the same delocalized vibrational state. Thus, a wide range of geometries around the conical intersection is spanned by the ground vibrational state wave function and the term *equilibrium configuration* is not applicable to cyclic-N_3 molecule. The splittings can indeed occur in the spectra, however, their origin is completely different and will be discussed in the last section of the paper.

Finally, Fig. 4 presents energies of the critical points in the neutral and ionic species as a function of the hyper-radius ρ, which can be pictured as the third internal coordinate perpendicular to the plane of Fig. 2. One can clearly see that both surfaces are rather anharmonic along this coordinate. Also, the minimum point, ρ_{MIN}, on PES of cyclic-N_3^+ occurs much earlier relative to the minimum energy point on neutral's PES. The corresponding zero-point energies are shown by the dashed lines and one can see that the Franck-Condon overlap with the vibrationally excited states of cyclic-N_3^+ should certainly be larger than the overlap with its ground vibrational state.

B. Vibrational structure of cyclic-N_3^+

Tables I–III present the lowest 64, 32, and 96 eigenvalues of symmetries A_1, A_2 and E, respectively (the latter are doubly degenerate). The energy origin is set at the bottom of the cyclic-N_3^+ well. The energy range extends up to

TABLE I. Energies, assignments, and Franck-Condon factors of the vibrational states of symmetry A_1 in cyclic-N_3^+ molecule.

No.	E (cm^{-1})	(v_1,v_2,v_3)	(v_1,v^ℓ)	FC[a]
1	1 927.48	(0,0,0)	$(0,0^0)$	5.64*E*−3
2	3 545.97	(1,0,0)	$(1,0^0)$	1.63*E*−2
3	4 112.04	(0,1,0)	$(0,2^0)$	4.36*E*−2
4	5 153.92	(2,0,0)	$(2,0^0)$	2.62*E*−2
5	5 174.06	(0,0,2)	$(0,3^{+3})$	1.79*E*−2
6	5 683.89	(1,1,0)	$(1,2^0)$	9.95*E*−2
7	6 277.00	(0,2,0)	$(0,4^0)$	5.37*E*−2
8	6 719.77	(1,0,2)	$(1,3^{+3})$	5.51*E*−2
9	6 753.65	(3,0,0)	$(3,0^0)$	6.97*E*−3
10	7 244.20	(2,1,0)	$(2,2^0)$	1.01*E*−1
11	7 329.81	(0,1,2)	$(0,5^{+3})$	1.36*E*−2
12	7 804.52	(1,2,0)	$(1,4^0)$	9.91*E*−2
13	8 253.80	(2,0,2)	$(2,3^{+3})$	4.12*E*−2
14	8 328.27	(0,0,4)	$(0,6^{+6})$	3.88*E*−3
15	8 342.99	(4,0,0)	$(4,0^0)$	4.17*E*−3
16	8 422.05	(0,3,0)	$(0,6^0)$	1.92*E*−2
17	8 791.75	(3,1,0)	$(3,2^0)$	7.35*E*−2
18	8 836.42	(1,1,2)	$(1,5^{+3})$	1.39*E*−2
19	9 321.56	(2,2,0)	$(2,4^0)$	7.67*E*−2
20	9 466.04	(0,2,2)	$(0,7^{+3})$	3.16*E*−3
21	9 769.95	(3,0,2)	$(3,3^{+3})$	1.56*E*−2
22	9 812.18	(1,0,4)	$(1,6^{+6})$	8.41*E*−3
23	9 907.60	(1,3,0)	$(1,6^0)$	2.68*E*−2
24	9 926.05	(5,0,0)	$(5,0^0)$	2.59*E*−3
25	10 316.66	(2,1,2)[b]	$(2,5^{+3})$	4.34*E*−2
26	10 348.23	(4,1,0)[b]	$(4,2^0)$	4.74*E*−4
27	10 452.36	(0,1,4)	$(0,8^{+6})$	1.45*E*−4
28	10 546.08	(0,4,0)	$(0,8^0)$	2.77*E*−3
29	10 831.69	(3,2,0)	$(3,4^0)$	3.75*E*−2
30	10 931.14	(1,2,2)	$(1,7^{+3})$	2.99*E*−3
31	11 253.24	(2,0,4)	$(2,6^{+6})$	1.80*E*−3
32	11 309.01	(4,0,2)	$(4,3^{+3})$	7.24*E*−3
33	11 387.44	(2,3,0)	$(2,6^0)$	1.67*E*−2
34	11 392.03	(0,0,6)	$(0,9^{+9})$	6.14*E*−7
35	11 506.37	(6,0,0)	$(6,0^0)$	6.74*E*−4
36	11 580.01	(0,3,2)	$(0,9^{+3})$	2.76*E*−4
37	11 810.77	(3,1,2)	$(3,5^{+3})$	1.30*E*−2
38	11 878.27	(5,1,0)	$(5,2^0)$	2.45*E*−3
39	11 899.09	(1,1,4)	$(1,8^{+6})$	8.07*E*−5
40	11 992.55	(1,4,0)	$(1,8^0)$	3.13*E*−3
41	12 333.48	(4,2,0)	$(4,4^0)$	1.42*E*−2
42	12 397.09	(2,2,2)	$(2,7^{+3})$	4.38*E*−4
43	12 555.84	(0,2,4)	$(0,10^{+6})$	3.78*E*−5
44	12 649.25	(0,5,0)	$(0,10^0)$	1.47*E*−4
45	12 713.05	(3,0,4)	$(3,6^{+6})$	2.62*E*−4
46	12 800.77	(5,0,2)[b]	$(5,3^{+3})$	8.03*E*−4
47	12 829.15	(1,0,6)[b]	$(1,9^{+9})$	2.50*E*−3
48	12 864.80	(3,3,0)	$(3,6^0)$	5.37*E*−3
49	13 008.66	(1,3,2)	$(1,9^{+3})$	2.18*E*−4
50	13 089.05	(7,0,0)	$(7,0^0)$	2.31*E*−4
51	13 282.51	(4,1,2)	$(4,5^{+3})$	2.66*E*−3
52	13 344.81	(2,1,4)	$(2,8^{+6})$	1.31*E*−3
53	13 420.53	(6,0,0)	$(6,2^0)$	2.55*E*−4
54	13 437.54	(2,4,0)	$(2,8^0)$	1.46*E*−3
55	13 483.41	(0,1,6)	$(0,11^{+9})$	3.02*E*−5
56	13 673.59	(0,4,2)	$(0,11^{+3})$	9.37*E*−6
57	13 814.16	(5,2,0)	$(5,4^0)$	3.81*E*−3
58	13 869.24	(3,2,2)[b]	$(3,7^{+3})$	6.05*E*−5
59	13 965.36	(1,2,4)	$(1,10^{+6})$	2.74*E*−5

TABLE I. (*Continued.*)

No.	E (cm^{-1})	(v_1,v_2,v_3)	(v_1,v^ℓ)	FC[a]
60	14 061.17	(1,5,0)	$(1,10^0)$	$1.29E-4$
61	14 151.21	(4,0,4)	$(4,6^{+6})$	$4.12E-5$
62	14 244.74	(2,0,6)[b]	$(2,9^{+9})$	$2.44E-5$
63	14 315.00	(4,3,0)[b]	$(4,6^0)$	$1.81E-3$
64	14 333.86	(2,3,2)[b]	$(2,9^{+3})$	$4.96E-4$

[a]The FC factors represent $\langle\psi_f|\psi_i\rangle^2$ in Eq. (9), where the initial wave function ψ_i describes the lowest state of symmetry A_1 in the neutral cyclic-N_3 molecule.
[b]The states with somewhat uncertain assignments. See text for details.

14 500 cm^{-1}. In addition to the symmetry labels, we employed two more approximate assignment methods described below.

The first method is based on counting the nodes of the vibrational wave functions along the hyperspherical coordinates ρ, θ, and ϕ. Although the hyperspherical coordinates are different from the normal mode coordinates, a displacement along the hyper-radius ρ is similar to the *symmetric stretch* of the triatomic molecule, while displacements along

TABLE II. Energies, assignments, and Franck-Condon factors of the vibrational states of A_2 symmetry in cyclic-N_3^+ molecule.

No.	E (cm^{-1})	(v_1,v_2,v_3)	(v_1,v^ℓ)	FC[a]
1	5 173.13	(0,0,1)	$(0,3^{-3})$	$9.71E-2$
2	6 719.93	(1,0,1)	$(1,3^{-3})$	$1.69E-1$
3	7 327.30	(0,1,1)	$(0,5^{-3})$	$7.60E-2$
4	8 253.43	(2,0,1)	$(2,3^{-3})$	$10.7E-1$
5	8 328.42	(0,0,3)	$(0,6^{-6})$	$4.62E-2$
6	8 830.89	(1,1,1)	$(1,5^{-3})$	$1.08E-1$
7	9 460.71	(0,2,1)	$(0,7^{-3})$	$1.79E-2$
8	9 769.29	(3,0,1)	$(3,3^{-3})$	$2.19E-2$
9	9 812.18	(1,0,3)	$(1,6^{-6})$	$5.63E-2$
10	10 324.71	(2,1,1)	$(2,5^{-3})$	$6.14E-2$
11	10 452.57	(0,1,3)	$(0,8^{-6})$	$3.27E-3$
12	10 923.81	(1,2,1)	$(1,7^{-3})$	$2.05E-2$
13	11 253.09	(2,0,3)	$(2,6^{-6})$	$4.16E-4$
14	11 308.78	(4,0,1)	$(4,3^{-3})$	$1.86E-2$
15	11 391.57	(0,0,5)	$(0,9^{-9})$	$3.04E-2$
16	11 573.2	(0,3,1)	$(0,9^{-3})$	$2.03E-3$
17	11 810.91	(3,1,1)	$(3,5^{-3})$	$2.00E-2$
18	11 895.52	(1,1,3)	$(1,8^{-6})$	$4.44E-3$
19	12 382.03	(2,2,1)	$(2,7^{-3})$	$9.32E-3$
20	12 554.12	(0,2,3)	$(0,10^{-6})$	$2.54E-4$
21	12 712.50	(3,0,3)[b]	$(3,6^{-6})$	$1.97E-4$
22	12 802.69	(5,0,1)[b]	$(5,3^{-3})$	$2.72E-4$
23	12 829.64	(1,0,5)[b]	$(1,9^{-9})$	$1.24E-2$
24	12 999.42	(1,3,1)	$(1,9^{-3})$	$1.65E-3$
25	13 279.71	(4,1,1)	$(4,5^{-3})$	$3.63E-3$
26	13 344.47	(2,1,3)	$(2,8^{-6})$	$3.29E-3$
27	13 483.76	(0,1,5)	$(0,11^{-9})$	$5.40E-5$
28	13 665.30	(0,4,1)	$(0,11^{-3})$	$6.08E-5$
29	13 832.72	(3,2,1)	$(3,7^{-3})$	$2.75E-3$
30	13 962.13	(1,2,3)	$(1,10^{-6})$	$2.10E-4$
31	14 149.88	(4,0,3)	$(4,6^{-6})$	$5.59E-5$
32	14 246.01	(6,0,1)	$(6,3^{-3})$	$4.10E-6$

[a]The FC factors represent $\langle\psi_f|\psi_i\rangle^2$ in Eq. (9), where the initial wave function ψ_i describes the lowest state of symmetry A_2 in the neutral.
[b]The states with somewhat uncertain assignments. See text for details.

TABLE III. Energies, assignments, and Franck-Condon factors of the vibrational states of E symmetry in cyclic-N_3^+ molecule.

No.	E (cm^{-1})	(v_1,v_2,v_3)	(v_1,v^ℓ)	FC[a]
1	3 019.41	(0,0,0)	$(0,1^{\pm1})$	$1.74E-2$
2	4 105.38	(0,0,1)	$(0,2^{\pm2})$	$6.62E-3$
3	4 614.40	(1,0,0)	$(1,1^{\pm1})$	$3.88E-2$
4	5 194.31	(0,1,0)	$(0,3^{\pm1})$	$4.03E-2$
5	5 676.25	(1,0,1)	$(1,2^{\pm2})$	$1.37E-2$
6	6 197.58	(2,0,0)	$(2,1^{\pm1})$	$3.57E-2$
7	6 235.48	(0,0,2)	$(0,4^{\pm4})$	$2.32E-3$
8	6 275.85	(0,1,1)	$(0,4^{\pm2})$	$7.43E-3$
9	6 743.52	(1,1,0)	$(1,3^{\pm1})$	$7.48E-2$
10	7 235.31	(2,0,1)	$(2,2^{\pm2})$	$1.14E-2$
11	7 287.49	(0,0,3)	$(0,5^{\pm5})$	$2.54E-3$
12	7 350.01	(0,2,0)	$(0,5^{\pm1})$	$2.24E-2$
13	7 754.66	(1,0,2)	$(1,4^{\pm4})$	$2.47E-3$
14	7 774.36	(3,0,0)	$(3,1^{\pm1})$	$2.33E-2$
15	7 802.91	(1,1,1)	$(1,4^{\pm2})$	$1.14E-2$
16	8 280.91	(2,1,0)	$(2,3^{\pm1})$	$5.80E-2$
17	8 380.85	(0,1,2)	$(0,6^{\pm4})$	$4.02E-4$
18	8 426.63	(0,2,1)	$(0,6^{\pm2})$	$2.55E-3$
19	8 772.70	(3,0,1)	$(3,2^{\pm2})$	$2.00E-3$
20	8 797.81	(1,0,3)	$(1,5^{\pm5})$	$7.49E-3$
21	8 856.39	(1,2,0)	$(1,5^{\pm1})$	$3.30E-2$
22	9 265.97	(2,0,2)	$(2,4^{\pm4})$	$2.78E-4$
23	9 316.67	(2,1,1)	$(2,4^{\pm2})$	$1.57E-2$
24	9 336.36	(4,0,0)	$(4,1^{\pm1})$	$3.66E-3$
25	9 359.50	(0,0,4)	$(0,7^{\pm7})$	$7.43E-4$
26	9 422.51	(0,1,3)	$(0,7^{\pm5})$	$2.91E-4$
27	9 486.02	(0,3,0)	$(0,7^{\pm1})$	$4.64E-3$
28	9 806.99	(3,1,0)	$(3,3^{\pm1})$	$2.71E-2$
29	9 864.58	(1,1,2)	$(1,6^{\pm4})$	$1.08E-3$
30	9 911.84	(1,2,1)	$(1,6^{\pm2})$	$3.25E-3$
31	10 266.28	(2,0,3)	$(2,5^{\pm5})$	$4.96E-5$
32	10 326.83	(4,0,1)	$(4,2^{\pm2})$	$6.05E-3$
33	10 355.39	(2,2,0)	$(2,5^{\pm1})$	$1.78E-2$
34	10 380.99	(0,0,5)	$(0,8^{\pm8})$	$1.10E-3$
35	10 505.53	(0,2,2)	$(0,8^{\pm4})$	$6.04E-5$
36	10 554.76	(0,3,1)	$(0,8^{\pm2})$	$3.30E-4$
37	10 759.55	(3,0,2)	$(3,4^{\pm4})$	$2.72E-4$
38	10 821.58	(1,0,4)	$(1,7^{\pm7})$	$3.71E-4$
39	10 823.55	(3,1,1)	$(3,4^{\pm2})$	$5.37E-3$
40	10 886.07	(1,1,3)	$(1,7^{\pm5})$	$1.89E-3$
41	10 890.99	(5,0,0)	$(5,1^{\pm1})$	$5.41E-4$
42	10 952.03	(1,3,0)	$(1,7^{\pm1})$	$5.51E-3$
43	11 317.8	(4,1,0)	$(4,3^{\pm1})$	$6.31E-3$
44	11 350.78	(2,1,2)	$(2,6^{\pm4})$	$3.92E-3$
45	11 392.13	(2,2,1)	$(2,6^{\pm2})$	$1.25E-3$
46	11 473.36	(0,1,4)	$(0,9^{\pm7})$	$6.78E-7$
47	11 537.85	(0,2,3)	$(0,9^{\pm5})$	$5.51E-5$
48	11 602.34	(0,4,0)	$(0,9^{\pm1})$	$3.90E-4$
49	11 740.67	(3,0,3)	$(3,5^{\pm5})$	$3.53E-5$
50	11 820.91	(1,0,5)	$(1,8^{\pm8})$	$1.35E-4$
51	11 843.55	(3,2,0)	$(3,5^{\pm1})$	$8.81E-3$
52	11 864.72	(5,0,1)	$(5,2^{\pm2})$	$2.96E-4$
53	11 950.38	(1,2,2)	$(1,8^{\pm4})$	$9.48E-5$
54	12 000.10	(1,3,1)	$(1,8^{\pm2})$	$3.44E-4$
55	12 229.50	(2,0,4)	$(2,7^{\pm7})$	$1.07E-4$
56	12 294.48	(4,0,2)	$(4,4^{\pm4})$	$9.59E-6$
57	12 311.71	(4,1,1)	$(4,4^{\pm2})$	$9.38E-4$
58	12 358.97	(2,1,3)	$(2,7^{\pm5})$	$1.36E-3$
59	12 392.94	(0,0,6)	$(0,10^{\pm10})$	$7.55E-4$

TABLE III. (*Continued.*)

No.	E (cm^{-1})	(v_1,v_2,v_3)	(v_1,v^ℓ)	FC[a]
60	12 414.60	(2,3,0)	$(2,7^{\pm1})$	2.08E−3
61	12 439.21	(6,0,0)	$(6,1^{\pm1})$	6.95E−4
62	12 483.52	(0,1,5)	$(0,10^{\pm8})$	8.76E−6
63	12 609.54	(0,3,2)[b]	$(0,10^{\pm4})$	2.70E−6
64	12 659.26	(0,4,1)	$(0,10^{\pm2})$	1.49E−5
65	12 796.12	(3,1,2)	$(3,6^{\pm4})$	5.20E−04
66	12 849.29	(5,1,0)[b]	$(5,3^{\pm1})$	2.48E−3
67	12 873.41	(3,2,1)[b]	$(3,6^{\pm2})$	5.38E−5
68	12 900.48	(1,1,4)	$(1,9^{\pm7})$	4.88E−5
69	12 964.48	(1,2,3)	$(1,9^{\pm5})$	5.91E−5
70	13 032.41	(1,4,0)	$(1,9^{\pm1})$	3.61E−4
71	13 195.36	(4,0,3)	$(4,5^{\pm5})$	1.24E−5
72	13 274.62	(2,0,5)	$(2,8^{\pm8})$	3.34E−6
73	13 327.78	(4,2,0)	$(4,5^{\pm1})$	2.45E−3
74	13 383.41	(0,0,7)[b]	$(0,11^{\pm11})$	2.66E−4
75	13 387.35	(6,0,1)[b]	$(6,2^{\pm2})$	6.33E−4
76	13 397.19	(2,2,2)	$(2,8^{\pm4})$	5.54E−5
77	13 444.95	(2,3,1)	$(2,8^{\pm2})$	1.12E−4
78	13 565.55	(0,2,4)	$(0,11^{\pm7})$	4.50E−6
79	13 632.50	(0,3,3)	$(0,11^{\pm5})$	1.06E−6
80	13 674.84	(3,0,4)	$(3,7^{\pm7})$	1.54E−5
81	13 700.93	(0,5,0)	$(0,11^{\pm1})$	1.45E−5
82	13 767.39	(3,1,3)	$(3,7^{\pm5})$	1.22E−4
83	13 768.38	(5,0,2)	$(5,4^{\pm4})$	2.62E−6
84	13 813.17	(1,0,6)	$(1,10^{\pm10})$	6.95E−5
85	13 838.28	(5,1,1)	$(5,4^{\pm2})$	6.86E−4
86	13 873.23	(3,3,0)	$(3,7^{\pm1})$	5.12E−4
87	13 895.88	(1,1,5)	$(1,10^{\pm8})$	9.97E−6
88	13 987.44	(7,0,0)	$(7,1^{\pm1})$	1.08E−4
89	14 019.44	(1,3,2)	$(1,10^{\pm4})$	3.66E−6
90	14 069.16	(1,4,1)	$(1,10^{\pm2})$	1.17E−5
91	14 243.43	(4,1,2)	$(4,6^{\pm4})$	5.19E−5
92	14 315.79	(4,2,1)	$(4,6^{\pm2})$	3.97E−4
93	14 325.64	(2,1,4)	$(2,9^{\pm7})$	5.69E−6
94	14 377.33	(6,0,0)	$(6,3^{\pm1})$	2.50E−4
95	14 397.51	(2,2,3)	$(2,9^{\pm5})$	4.65E−6
96	14 461.01	(2,4,0)	$(2,9^{\pm1})$	1.05E−4

[a]The FC factors are calculated according to Eq. (10).
[b]The states with somewhat uncertain assignments. See text for details.

the hyperangles θ and ϕ correspond to the *bend* and *asymmetric stretch*, respectively. The 3D vibrational wave functions for all the calculated states were plotted and are available for download as EPAPS.[36] Using these 3D plots, we assigned vibrational normal mode quantum numbers to all the calculated states. Those assignments are given as (v_1,v_2,v_3)=(symmetric stretch, bend, asymmetric stretch) in all the figures in EPAPS, in Figs. 5 and 6 below, as well as in the third column in Tables I–III. The states of A_1 symmetry are labeled only by even v_3, whereas the states of A_2 symmetry are labeled only by odd v_3. The states of E symmetry are labeled by both even and odd v_3.

We will now discuss the nodal structure of the vibrational wave functions of cyclic-N_3^+. Figures 5 and 6 present several typical examples, which employ 3D isosurfaces in the hyperspherical coordinates[6,7] (a diagram is given in the top portion of Fig. 5 to facilitate the analysis). The lowest energy vibrational state is the ground A_1 state at

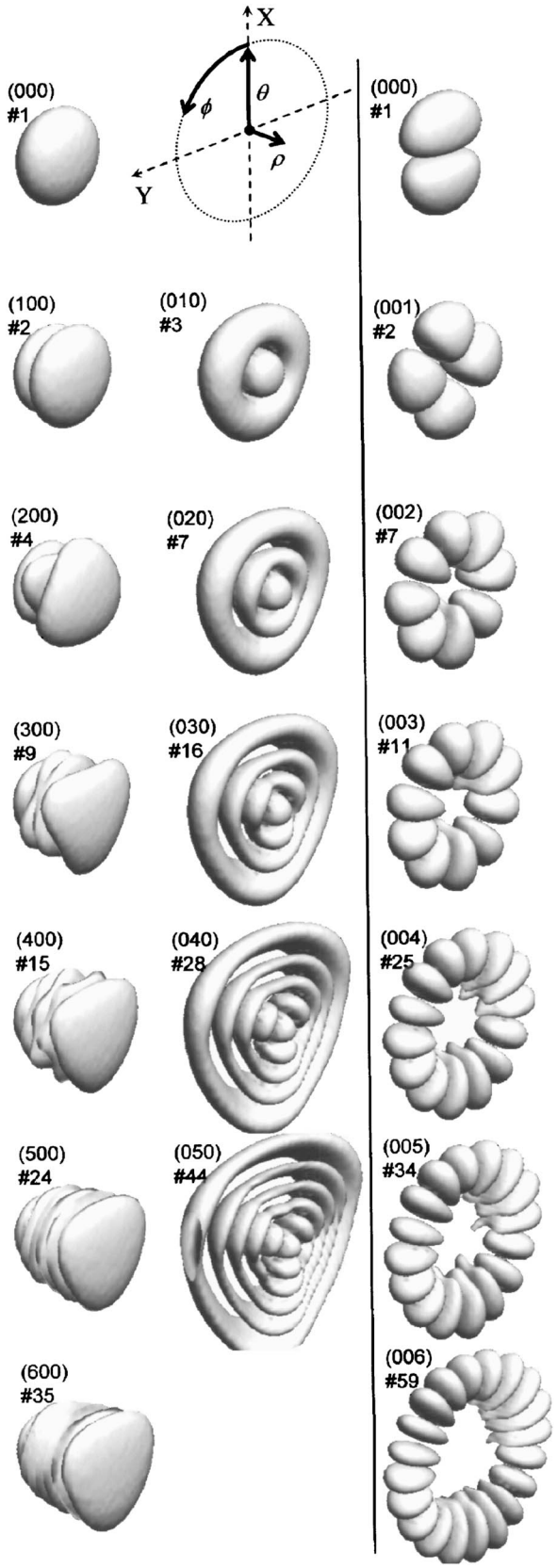

FIG. 5. 3D wave functions for several vibrational states of cyclic-N_3^+. The state number and its assignment in terms of (v_1,v_2,v_3) are given for each state. First column: progression of v_1 states of A_1 symmetry; second column: progression of v_2 states of A_1 symmetry; third column: progression of v_3 states of E symmetry. Schematic in the top of the figure is given to facilitate analysis of the nodal structure. The hyper-radial direction ρ is plotted perpendicularly to the (X,Y) plane. Isovalue surfaces are plotted through the points with $|\psi|^2$=0.1.

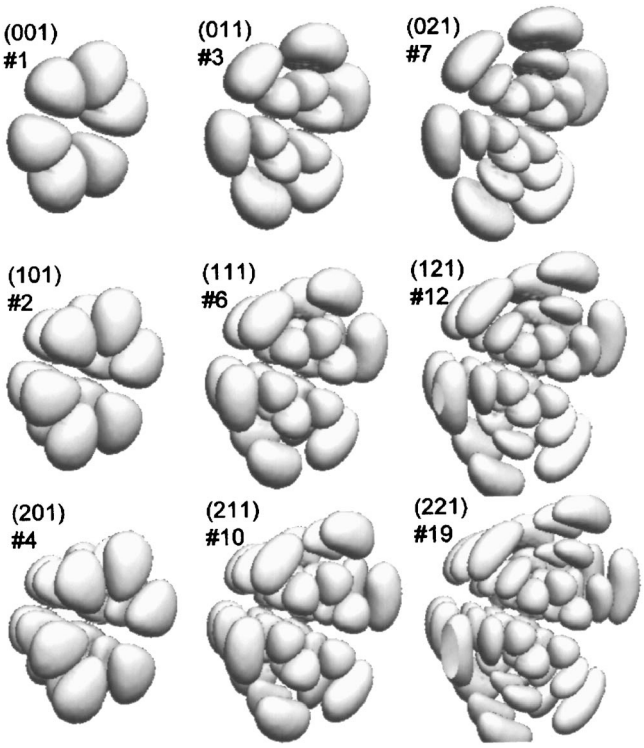

FIG. 6. 3D wave functions for several vibrational states of cyclic-N_3^+. A two-dimensional progression of combination states of A_2 symmetry is shown. Assignments and nodal structure analysis are as in Fig. 5. See text for discussion.

1927.48 cm^{-1} assigned as (0,0,0). There are no nodes in the ground state wave function, i.e., it is basically a 3D Gaussian. The first column in Fig. 5 shows a long progression of $(v_1,0,0)$ states of A_1 symmetry with $0 \leqslant v_1 \leqslant 6$. Excitation of the symmetric stretch produces nodes along the hyper-radius and forces the wave functions to extend into the ranges of small and large values of ρ; however, they still remain localized around the $\theta=0$ line. The shapes of the wave functions in this progression remain regular through the entire range studied here. The wave function of the last of these states, (6,0,0) at 11 506.4 cm^{-1}, looks like a set of seven thin layers positioned perpendicularly to the hyper-radius ρ. Anisotropy along the hyperangle ϕ becomes already visible in the wave function of the (2,0,0) state at 5153.92 cm^{-1} as a distortion from the Gaussian-type shape towards a more triangular shape.

The second column in Fig. 5 shows a progression of the bending states $(0,v_2,0)$ of A_1 symmetry with $0 \leqslant v_2 \leqslant 5$. Excitation of this mode produces nodes along the hyperangle θ, which appear in 3D as concentric cylindrical nodal surfaces perpendicular to the (X,Y) plane. These nodes push the wave function out into the range of large θ where PES is very anharmonic. As excitation increases, the shapes of these wave functions remain regular but start to exhibit a lot of structure.

Finally, the third column in Fig. 5 shows a progression of asymmetric stretching states $(0,0,v_3)$ of E symmetry with $0 \leqslant v_3 \leqslant 6$. This progression exhibits the increasing number of nodes along the hyperangle ϕ and a very regular behavior of the wave functions. Interestingly, as v_3 increases, the wave functions in this progression move towards larger values of θ and at large values of v_3 an "empty space" is produced in the vicinity of the origin ($\theta=0$). Also, the wave functions of both bending and asymmetric stretching states (the second and third columns in Fig. 5) remain localized near the equilibrium value ρ_{eq} of the hyper-radius, expanding only into the (θ,ϕ) plane.

An example of the combination bands is illustrated in Fig. 6 using nine $(v_1,v_2,1)$ wave functions of A_2 symmetry with $0 \leqslant v_1 \leqslant 2$ and $0 \leqslant v_2 \leqslant 2$. The (0,0,1) state is the lowest A_2 state and its wave function exhibits only six nodes along ϕ, as required by symmetry, since it should be antisymmetric with respect to reflections through the $\phi=0$, $\phi=120°$, and $\phi=240°$ planes. Other wave functions in Fig. 6 feature superposition of these nodes with the nodes in θ and ρ. Even the wave function of the most complex state shown here, (2,2,1), shows very clean regular nodal structure in all three dimensions.

Based on these 3D plots, the (v_1,v_2,v_3) assignments are straightforward for almost all the states except a few, in which the structure of the vibrational wave function is complicated by intermode couplings and/or interactions with other states. Usually, such "difficult" states appear in the groups of two or three consecutive states with the same v_2 and equal values of v_1+v_3. Examples among the states of A_1 symmetry include #25 (2,1,2) and 26 (4,1,0); #46 (5,0,2) and 47 (1,0,6); and #63 (4,3,0) and 64 (2,3,2). Among the states of A_2 symmetry are #21 (3,0,3), 22 (5,0,1), and 23 (1,0,5); and #31 (4,0,3) and 32 (6,0,1). Among the states of E symmetry are #74 (0,0,7) and 75 (6,0,1) and some other states. This happens because in cyclic-N_3^+ the energy of one quantum of excitation in v_1 is very close to the energy of one quantum of excitation in v_3. Analysis of several lower states in Tables I–III reveals that the energy difference of such quanta varies (depending on symmetry) between only ~5 and 30 cm^{-1}. This complicates the assignments of the spectra. Moreover, the assignment based on the energy quanta is not very successful in these cases either, although the visual representation is still useful, even though the assignment is not immediately obvious. Assignments of the vibrational states in terms of polyads (as described below) were quite useful in such complicated cases.

The assignment in terms of (v_1,v_2,v_3) is straightforward to implement because our calculations were carried out in the same hyperspherical coordinates. Moreover, this assignment method enables direct comparison between the vibrational wave functions of cyclic N_3^+ and N_3. This assignment method is particularly useful (and sufficient) for any C_{2v} triatomic molecule with three deep, almost independent wells, when (i) the vibrational states of E symmetry become degenerate with the corresponding states of A_1 or A_2 symmetry and (ii) the vibrational wave functions become naturally localized in the three wells (centered at $\phi=0$, $\phi=120°$, and $\phi=240°$) and the number of nodes along ϕ over each well (i.e., for each independent isomer) has a usual meaning and is equal to the quantum number v_3. However, even in the previous study of cyclic-N_3, this method has been shown to be not quite adequate because the large splittings between the states of E and A_1 or A_2 symmetries (due to pseudorotation) led to re-

peating of the same (v_1,v_2,v_3) assignments (A_1, A_2, or E) were necessary in addition to the normal mode assignments. We also found that counting the nodes over the single cyclic-N_3 well is not convenient due to delocalization of the vibrational wave functions over the three wells and the global nature of their nodal structures. In fact, this classification scheme is even less appropriate for cyclic-N_3^+ that has a simple D_{3h} well almost isotropic along ϕ, and we had to include one more assignment method.

The vibrational states of the D_{3h} homonuclear triatomic molecules are often assigned in terms of triads[19–22,26,27] or, more generally, polyads. The first vibration mode in this assignment method is the same symmetric stretch mode characterized by the same quantum number v_1. Then it is assumed that the two other modes are degenerate and the energy levels (to the first order) can be described by

$$E^{(1)} = \omega_1\left(v_1 + \tfrac{1}{2}\right) + \omega(v+1), \tag{11}$$

where ω is the degenerate frequency and v is the composite quantum number, which gives the total number of vibration quanta in the two degenerate vibration modes. The third quantum number ℓ, which assumes values $-v \leqslant \ell \leqslant v$, is introduced to show how many of these quanta contribute to the vibrational angular momentum (pseudorotation). Thus, the vibrational states of cyclic-N_3^+ can be assigned in terms of the polyads (v_1,v^{ℓ}) where the states with the same v_1 and v but different values of ℓ are said to belong to the same polyad. The number ℓ takes values $\{-v,-v+2,\ldots,v-2,v\}$ and each polyad therefore contains $v+1$ states.

Even though this assignment method is also approximate, it has an advantage of producing unique labels for all states of all symmetries because ℓ determines the symmetry of the wave function. Namely, any two states with the same $|\ell| \neq 3k$ (k is integer or zero) constitute a strictly degenerate pair of E-symmetry states. The "+" and "−" signs denote symmetric and antisymmetric states, respectively. The states with $|\ell|=3k$ transform according to A symmetry, with the "+" sign used for symmetric (A_1-symmetry) states and the "−" sign for antisymmetric (A_2-symmetry) states. Since the pseudorotation motion occurs along the hyperangle ϕ, the positive number $|\ell|$ gives the number of nodal surfaces and $2\times|\ell|$ gives the number of nodes found along ϕ in the entire physical range of $0 \leqslant \phi \leqslant 360°$. This method can be used even if PES is not purely harmonic and the two vibration modes are not exactly degenerate; however, some splitting between the different ℓ states will be observed. When anharmonicities are taken into account to the second order of perturbation theory,[56] the energy spectrum is described by

$$E^{(2)} = \omega_1\left(v_1 + \tfrac{1}{2}\right) + \omega(v+1) + \delta_1\left(v_1 + \tfrac{1}{2}\right)^2 + \delta(v+1)^2 + \Delta\left(v_1 + \tfrac{1}{2}\right)(v+1) + g(\ell)^2. \tag{12}$$

The above expression has a second order dependence on $|\ell|$, but no dependence on the sign of ℓ (i.e., no splitting between the states of A_1 and A_2 symmetries).

Having assigned all the states of A_1, A_2, and E symmetries in terms of (v_1,v_2,v_3), it is now straightforward to assign all the states in terms of (v_1,v^{ℓ}). These assignments are given in the fourth column of each table and in all the figures in the EPAPS submission.[36] Also included with the EPAPS submission. is the table in which all the states of all symmetries are combined and arranged according to the polyads (i.e., the states with the same v_1 and v are grouped together), to simplify data analysis and fitting.

Below we describe the major features of the vibrational spectra in the cyclic-N_3^+. The spacing between the vibrational polyads is rather large. In the energy range studied here, different polyads with the same quantum number v_1 do not overlap; different polyads with the same quantum number v do not overlap either. Neighboring polyads with the same total number of quanta v_1+v and $\Delta v_1=\Delta v=1$ do not overlap too. The first overlap is found between the (3,1) polyad at 7774.4 cm^{-1} and (1,4) polyad. The next one is between (4,0) polyad at 8343.0 cm^{-1} and (0,6) polyad. Several more examples of this kind, when a (large v_1, small v) polyad overlaps with a (small v_1, large v) polyad, can be found above 10 000 cm^{-1}. Within the polyads, energies of the vibrational states drop as $|\ell|$ increases in most cases. This suggests that in cyclic-N_3^+ excitation of the bending motion requires slightly less energy than the excitation of the pseudorotational motion. Exceptions to this rule are found only in the polyads with $v=6$, 8, and 10; there the $\ell=0$ states are always below the $\ell\pm2$ states.

Within the polyads, splittings between the states with equal values of $|\ell|$ but opposite signs are relatively small and are less or about 1 cm^{-1} in most cases. Only a few exceptions are found at energies above 10 000 cm^{-1}. For example, splittings of about 10 cm^{-1} are found between $(2,5^{-3})$ and $(2,5^{+3})$, $(1,9^{-3})$ and $(1,9^{+3})$, and $(0,11^{-3})$ and $(0,11^{+3})$ states. The two largest splittings of this kind are 15.0 cm^{-1} between $(2,7^{-3})$ and $(2,7^{+3})$ states, and 36.5 cm^{-1} between $(3,7^{-3})$ and $(3,7^{+3})$ states; however, these pairs lie at relatively high energies: 12 382.0 and 13 832.7 cm^{-1}, respectively. Furthermore, the $(3,7^{+3})$ state is among those states that were difficult to assign due to its mixing with other states, which partially explains such a large splitting. Note that this kind of splitting occurs between the states of A_1 and A_2 symmetries, which have the same number of quanta of every kind and the same number of nodes along each coordinate. The difference is that at $\phi=0$, 120°, and 240° the wave functions of A_1 symmetry exhibit maxima, whereas those of A_2 symmetry exhibit nodes. Thus, the overall shapes of the wave functions are very similar, however, one is rotated by $\Delta\phi=60°$ with respect to another [see EPAPS (Ref. 36)]. If PES were exactly isotropic along the hyperangle ϕ the wave functions would yield equal expectation values for energies, but some ϕ dependence in PES results in small splitting of these states. Note that this kind of splitting is not present in the spectrum of Eq. (12).

Within the polyads, splittings between the states with different $|\ell|$ are somewhat larger. The lowest energy example is a splitting of 6.7 cm^{-1} between $(0,2^0)$ state and $(0,2^{\pm2})$ exactly degenerate state. Remember that the first of these states is of A_1 symmetry and the second state is of E symmetry. Their wave functions exhibit very different nodal structures [see EPAPS (Ref. 36)] and this splitting is not surprising, even at low energies. The splitting can even be

larger when the same polyad contains two (or more) consecutive states of the same symmetry. The lowest energy example of this kind is a splitting of 40.4 cm^{-1} between $(0,4^{\pm 2})$ and $(0,4^{\pm 4})$ states of E symmetry at 6235.5 cm^{-1}. The first example of three consecutive states of E symmetry occurs in (0,7) polyad, and so on. For many polyads at energies near 10 000 cm^{-1} the values of such splittings average at 50 cm^{-1} and exceed 100 cm^{-1} for several higher energy polyads.

Splittings of the latter kind (i.e., between the states with different $|\ell|$) can be reproduced by an approximate spectrum of Eq. (12) and we used this formula to fit our results. We fitted only a part of the spectrum below 10 000 cm^{-1}; this includes 63 states of all symmetries, which constitute 27 lowest energy polyads. No weighting function was used. Results of the fit for frequencies and anharmonicities in Eq. (12) are $\omega_1=1654.95$ cm^{-1}, $\omega=1114.18$ cm^{-1}, $\delta_1=-5.53$ cm^{-1}, $\delta=-2.31$ cm^{-1}, $\Delta=-23.94$ cm^{-1}, and $g=-2.76$ cm^{-1}. The standard deviation of the fit was 6.13 cm^{-1}. One could expect that the symmetric stretching mode is more anharmonic, however the fit shows that both intramode anharmonicities (δ_1 and δ) are relatively small for this molecule. The pseudorotational anharmonicity parameter g is also small. However, the fitted value of the intermode anharmonicity Δ is found to be quite large. These data can be used for qualitative analysis of the spectra.

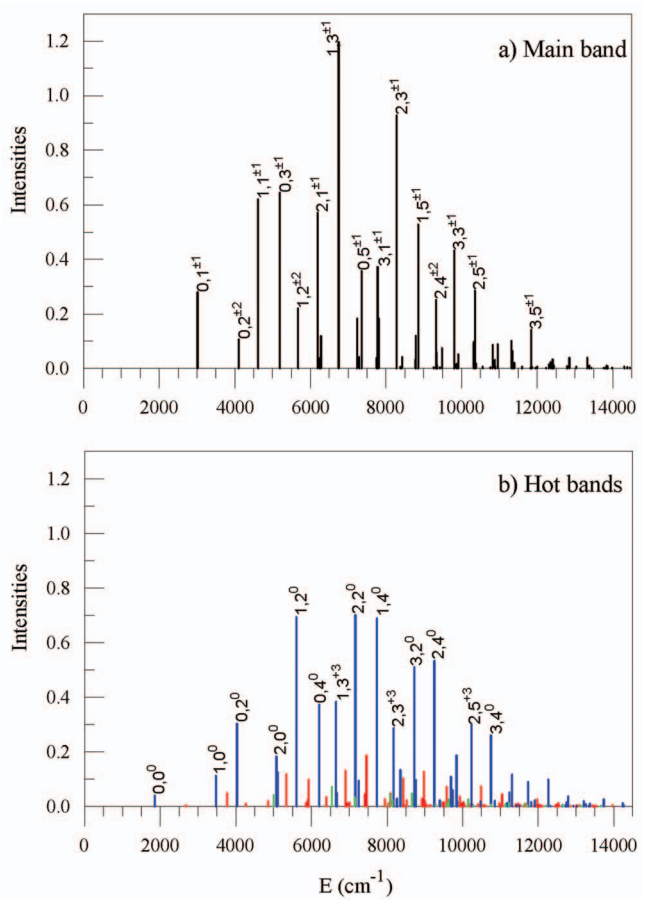

FIG. 7. (Color) Theoretically predicted photoelectron spectra of cyclic-N_3. (a) Main band of $E' \rightarrow E''$ transitions; (b) hot bands of $A_1' \rightarrow A_1''$ transitions (blue), $A_2' \rightarrow A_2''$ transitions (green), and $E' \rightarrow E''$ transitions (red). See text for description of the initial states. Final state labels in terms of polyads (v_1, v^ℓ) are given for several most intense peaks.

C. Photoelectron spectra of cyclic-N_3

The fifth column of Tables I–III summarizes the FC factors. Their analysis is rather straightforward: The largest factors occur for those final states ψ_f characterized by small quantum number ℓ. For example, among the states of A_1 symmetry these are $(1,2^0)$, $(2,2^0)$, and $(1,4^0)$; among the states of A_2 symmetry we find larger factors for $(1,3^{-3})$, $(2,3^{-3})$, and $(1,5^{-3})$; among the E-symmetry states, for $(0,3^{\pm 1})$, $(1,3^{\pm 1})$, and $(2,3^{\pm 1})$. This is simply because the initial states ψ_i of the neutral cyclic-N_3 are also characterized by small quantum number ℓ: in terms of the polyads they would be assigned as $(0,0^0)$, $(0,3^{-3})$, and $(0,1^{\pm 1})$. These are the lowest states of A_1, A_2, and E symmetries, respectively, and their wave functions contain the minimal number of nodes in ϕ. More ϕ nodes in the final state leads to significant cancellations in the integral over ϕ in Eq. (9) and results in a smaller overlap. The largest FC factor is 0.169 for state $(1,3^{-3})$ of A_2 symmetry. More than ten other FC factors approach 0.1 and the corresponding states always lie in the energy range between 5000 and 10 000 cm^{-1}. Also, note that such states most often contain one or two quanta of v_1 required to reach the favorable Franck-Condon region in ρ, as also follows from Fig. 4.

Figure 7(a) shows intensities of the main $E' \rightarrow E''$ band of the photoelectron spectrum. The reference point (zero) in this plot corresponds to the minimum energy point of PES for ionic cyclic-N_3^+, which is 10.356 eV above the ground vibrational state of neutral cyclic-N_3. A nice progression of $\ell=\pm 1$ states can be easily identified:

$(0,1^{\pm 1})$, $(0,3^{\pm 1})$, $(0,5^{\pm 1})$;

$(1,1^{\pm 1})$, $(1,3^{\pm 1})$, $(1,5^{\pm 1})$;

$(2,1^{\pm 1})$, $(2,3^{\pm 1})$, $(2,5^{\pm 1})$;

$(3,1^{\pm 1})$, $(3,3^{\pm 1})$, $(3,5^{\pm 1})$;

as well as several less intense $\ell=\pm 2$ states:

$(0,2^{\pm 2})$, $(0,4^{\pm 2})$;

$(1,2^{\pm 2})$, $(1,4^{\pm 2})$;

$(2,2^{\pm 2})$, $(2,4^{\pm 2})$.

These progressions should be clearly seen in the experiment. The most intense peak corresponds to $(1,3^{\pm 1})$ state with no other peaks within about ±500 cm^{-1}. The vibrational wave function of this final state is shown in Fig. 1, along with the wave function of the initial, ground vibrational state of cyclic-N_3. All other intense peaks at energies above 6000 cm^{-1} are surrounded by several relatively close less intense peaks, which most often originate from E-symmetry states of the same polyad with $\ell=\pm 2$ or larger (although sometimes from the states of other energetically close poly-

ads). In the experiment, where apparatus broadening is present, this group of peaks can appear as a broader peak with several splittings. Due to uncertainties in the electronic structure calculations (about 2%, as suggested by the error bars for harmonic frequencies), these progressions may shift relative to each other. However, since the separations between the main peaks are about 500 cm^{-1}, even the shifts of about 100 cm^{-1} will not cause qualitative changes in the spectrum.

Note that the broad spectrum of cyclic-N_3 [Fig. 7(a)] differs dramatically from that of the linear trinitrogen isomer,[57,58] which has only one intense peak in this energy range because of the similarity in the equilibrium structures of the neutral and ionized species. On the scale of Fig. 7(a) this single peak would appear at about 5680 cm^{-1}.[57,59] The ionization potential (IP) of the linear isomer is 11.06 eV,[57] which is 0.44 eV higher than the IP of the cyclic form.[14] These differences in IP and the shape of the photoelectron spectra should help to distinguish the two isomers simultaneously present in the experimental molecular beam.[1–3,9–11]

Further complexity in the photoelectron spectrum of cyclic-N_3 is brought by its hot bands: $A_1' \rightarrow A_1''$ and $A_2' \rightarrow A_2''$ and the hot $E' \rightarrow E''$, shown collectively in Fig. 7(b). Here the most intense peaks belong to the coldest $A_1' \rightarrow A_1''$ band. Among them the most pronounced are the $\ell = 0$ peaks:

$(0,2^0)$, $(0,4^0)$;

$(1,2^0)$, $(1,4^0)$, $(1,6^0)$;

$(2,2^0)$, $(2,4^0)$;

but also several $\ell = +3$ peaks:

$(0,3^{+3})$, $(0,5^{+3})$;

$(1,3^{+3})$, $(1,5^{+3})$;

$(2,3^{+3})$, $(2,5^{+3})$.

Due to the low nuclear spin factor the peaks of $A_2' \rightarrow A_2''$ band are even less intense than the peaks of the hotter $E' \rightarrow E''$ band. Since the initial state for this hot E band is the first excited state of E symmetry in cyclic-N_3 assigned as $(0,2^{\pm 2})$, the most intense peaks here describe transitions to $\ell = \pm 2$ states of cyclic-N_3^+. This is the same progression of $\ell = \pm 2$ states given above, although the peaks of the hot bands do not occur near the peaks of the cold band, which belong to the same polyad, as they are shifted by the vibrational excitation energy of the initial vibrational states in the cyclic-N_3. If both frames of Fig. 7 are superimposed, the resulting spectrum (192 peaks total) becomes rather complicated. This suggests that it would be much easier to identify the cyclic-N_3 molecules in the experiment where these molecules are produced vibrationally cold and are spectroscopically characterized while they remain cold, so that only the main $E' \rightarrow E''$ band of Fig. 7(a) is observed.

IV. CONCLUSIONS

We presented PES and vibrational wave functions of cyclic-N_3^+. High level *ab initio* calculations were carried out to obtain energies of the points on a three-dimensional grid and a spline interpolation of these data was used to construct accurate representation of the potential energy surface employing hyperspherical coordinates. The vibrational state energies and wave functions were calculated in the energy range up to 14 500 cm^{-1}, taking into account all couplings present in PES and full dimensionality of the problem. All the states were assigned and the spectrum was fitted with a simple analytic expression for the vibrational polyads. To predict intensities in the photoelectron spectrum of cyclic-N_3, the Franck-Condon overlaps were computed between these states and several low energy states of the neutral cyclic-N_3. The geometric phase effects in cyclic-N_3 were included by using the initial vibrational wave functions obtained from the gauge theory. The most important consequence of the geometric phase is the reversal of state symmetries and appearance of $E' \rightarrow E''$ transitions in the main photoelectron band, with $A_1' \rightarrow A_1''$ transitions forming the most intense of hot bands. Intensities of the photoelectron peaks reflect the nodal structure of the initial and final vibrational wave functions.

The photoelectron spectra of cyclic-N_3 should provide the structural information about both species: neutral cyclic-N_3 and ionic cyclic-N_3^+, due to the fact that several low lying vibrational states of cyclic-N_3 molecule are populated in the experimental conditions and the hot bands are produced when those states are photoionized. Theoretical predictions of the peak intensities reported here should facilitate the analysis of the experimental results.

From the theory perspective, this work suggests further developments. First of all, predictions of peak intensities could be refined by computing the dipole moment function and using the first expression of Eq. (9), in order to fully incorporate the geometric phase effects in the spectrum calculations. Similar calculations of the *infrared* line intensities of cyclic-N_3 are underway.[13] Moreover, the excited electronic states of cyclic-N_3^+ that lie in the range of 5–8 eV above the energy of the ground electronic state[14] can be included in the modeling of the spectrum as well. We plan to pursue such calculations in the future.

ACKNOWLEDGMENTS

Brian Kendrick in Los Alamos National Laboratory is gratefully acknowledged for sharing his hyper-spherical code. One of the authors (D.B.) is very thankful to Scott Reid in Marquette University for numerous discussions. This research was partially supported by NSF Grant No. PHY-045953. It also used resources of the National Energy Research Scientific Computing Center, supported by the Office of Science of the U.S. Department of Energy under Contract No. DE-AC03-76SF00098. Another author (A.I.K.) acknowledges the support from the Department of Energy (DE-FG02-05ER15685) and University of Southern California Center for High Performance Computing and Communications for making their computational resources available.

[1] N. Hansen and A. M. Wodtke, J. Phys. Chem. A **107**, 10608 (2003).
[2] N. Hansen, A. M. Wodtke, A. V. Komissarov, K. Morokuma, and M. C. Heaven, J. Chem. Phys. **118**, 10485 (2003).

[3] M. Wodtke, N. Hansen, J. C. Robinson, N. E. Sveum, S. J. Goncher, and D. M. Neumark, Chem. Phys. Lett. **391**, 334 (2004).
[4] M. Bittererova, H. Ostmark, and T. Brink, J. Chem. Phys. **116**, 9740 (2002).
[5] P. Zhang, K. Morokuma, and A. M. Wodtke, J. Chem. Phys. **122**, 14106 (2005).
[6] D. Babikov, P. Zhang, and K. Morokuma, J. Chem. Phys. **121**, 6743 (2004).
[7] D. Babikov, B. Kendrick, P. Zhang, and K. Morokuma, J. Chem. Phys. **122**, 44315 (2005).
[8] J. Zhang, Y. Chen, K. Yuan, S. A. Harich, X. Wang, X. Yang, P. Zhang, Z. Wang, K. Morokuma, and A. M. Wodtke, Phys. Chem. Chem. Phys. **8**, 1690 (2006).
[9] N. Hansen, A. M. Wodtke, S. J. Goncher, J. C. Robinson, N. E. Sveum, and D. M. Neumark, J. Chem. Phys. **123**, 104305 (2005).
[10] P. C. Samartzis, J. J. M. Lin, T. T. Ching, C. Chaudhuri, Y. T. Lee, S. H. Lee, and A. M. Wodtke, J. Chem. Phys. **123**, 51101 (2005).
[11] P. C. Samartzis, N. Hansen, and A. M. Wodtke, Phys. Chem. Chem. Phys. **8**, 2958 (2006).
[12] P. C. Samartzis and A. M. Wodtke, Int. Rev. Phys. Chem. (to be published).
[13] D. Babikov, B. Kendrick, P. Zhang, and K. Morokuma (unpublished).
[14] V. A. Mozhayskiy, D. Babikov, and A. I. Krylov, J. Chem. Phys. **124**, 224309 (2006).
[15] S. Carter and W. Meyer, J. Chem. Phys. **93**, 8902 (1990).
[16] W. Meyer, P. Botschwina, and P. Burton, J. Chem. Phys. **84**, 891 (1986).
[17] R. M. Whitnell and J. C. Light, J. Chem. Phys. **90**, 1774 (1989).
[18] D. A. Sadovskii, N. G. Fulton, J. R. Henderson, J. Tennyson, and B. I. Zhilinskii, J. Chem. Phys. **99**, 906 (1993).
[19] V. Kokoouline, C. H. Greene, and B. D. Esry, Nature (London) **412**, 891 (2001).
[20] V. Kokoouline and C. H. Greene, Phys. Rev. A **68**, 12703 (2003).
[21] V. Kokoouline and C. H. Greene, Phys. Rev. A **69**, 32711 (2004).
[22] H.-G. Krämer, M. Keil, C. B. Suarez, W. Demtröder, and W. Meyer, Chem. Phys. Lett. **299**, 212 (1999).
[23] M. Keil, H.-G. Krämer, A. Kudell, M. A. Baig, J. Zhu, W. Demtröder, and W. Meyer, J. Chem. Phys. **113**, 7414 (2000).
[24] P. Cias, M. Araki, A. Denisov, and J. P. Maier, J. Chem. Phys. **121**, 6776 (2004).
[25] A. M. Mebel and R. I. Kaiser, Chem. Phys. Lett. **360**, 139 (2002), and references therein.
[26] R. Siebert and R. Schinke, J. Chem. Phys. **119**, 3092 (2003).
[27] Z.-W. Qu, H. Zhu, and R. Schinke, J. Chem. Phys. **123**, 204324 (2005).
[28] R. T Pack and G. A. Parker, J. Chem. Phys. **87**, 3888 (1987).
[29] B. K. Kendrick, R. T Pack, R. B. Walker, and E. F. Hayes, J. Chem. Phys. **110**, 6673 (1999), and references therein.
[30] H. Koch, H. Jørgen Aa. Jensen, P. Jørgensen, and T. Helgaker, J. Chem. Phys. **93**, 3345 (1990).
[31] J. F. Stanton and R. J. Bartlett, J. Chem. Phys. **98**, 7029 (1993).
[32] S. V. Levchenko and A. I. Krylov, J. Chem. Phys. **120**, 175 (2004).
[33] T. H. Dunning, J. Chem. Phys. **90**, 1007 (1989).
[34] J. Kong, C. A. White, A. I. Krylov *et al.*, J. Comput. Chem. **21**, 1532 (2000).
[35] F. Pawłowski, A. Halkier, P. Jørgensen, K. L. Bak, T. Helgaker, and W. Klopper, J. Chem. Phys. **118**, 2539 (2003).
[36] See EPAPS Document No. E-JCPSA6-125-306632 for *ab initio* data, for 3D wave functions of all the vibrational states in cyclic-N_3^+ and for the assignments of these states in terms of polyads. This document can be reached via a direct link in the online article's HTML reference section or via the EPAPS homepage (http://www.aip.org/pubservs/epaps.html).
[37] C. de Boor, *A Practical Guide to Splines* (Springer, New York, 1978).
[38] B. K. Kendrick, Phys. Rev. Lett. **79**, 2431 (1997).
[39] B. K. Kendrick, Int. J. Quantum Chem. **64**, 581 (1997).
[40] B. K. Kendrick and R. T Pack, J. Chem. Phys. **106**, 3519 (1997).
[41] B. K. Kendrick and R. T Pack, J. Chem. Phys. **104**, 7475 (1996).
[42] B. R. Johnson, J. Chem. Phys. **67**, 4086 (1977); *ibid.* **69**, 4678 (1978).
[43] J. Simons, *An Introduction to Theoretical Chemistry* (Cambridge University Press, Cambridge, UK, 2003).
[44] M. V. Berry, Proc. R. Soc. London, Ser. A **392**, 45 (1984).
[45] B. K. Kendrick, Int. J. Quantum Chem. **64**, 581 (1997).
[46] B. K. Kendrick, in *Geometric Phase Effects in Chemical Reaction Dynamics*, Conical Intersections: Electronic Structure, Dynamics and Spectroscopy Vol. 15, edited by W. Domcke, D. R. Yarkony, and H. Köppel (World Scientific, Singapore, 2004).
[47] B. Lepetit and A. Kuppermann, Chem. Phys. Lett. **166**, 581 (1990).
[48] Y. S. M. Wu, A. Kuperman, and B. Lepetit, Chem. Phys. Lett. **186**, 319 (1991).
[49] C. A. Mead and D. G. Truhlar, J. Chem. Phys. **70**, 2284 (1979); C. A. Mead, *ibid.* **72**, 3839 (1980).
[50] C. A. Mead, Chem. Phys. **49**, 23 (1980).
[51] T. C. Thompson, D. G. Truhlar, and C. A. Mead, J. Chem. Phys. **82**, 2392 (1985).
[52] D. G. Truhlar, T. C. Thompson, and C. A. Mead, Chem. Phys. Lett. **127**, 287 (1986).
[53] P. Garcia-Fernandez, I. B. Bersuker, and J. E. Boggs, Phys. Rev. Lett. **96**, 163005 (2006).
[54] J. H. D. Eland, *Photoelectron Spectroscopy* (Wiley, New York, 1974).
[55] R. E. Ballard, *Photoelectron Spectroscopy and Molecular Orbital Theory* (Hilger, Bristol, 1978).
[56] G. D. Carney, S. M. Adler-Golden, and D. C. Lesseski, J. Chem. Phys. **84**, 3921 (1986).
[57] J. M. Dyke, N. B. Jonathan, A. E. Lewis, and A. Moris, Mol. Phys. **47**, 1231 (1982).
[58] R. Tarroni and P. Tosi, Chem. Phys. Lett. **389**, 274 (2004).
[59] V. A. Mozhayskiy, D. Babikov, and A. I. Krylov J. Chem. Phys. **124**, 224309 (2006).